Skin Heating and Injury by Prolonged Millimeter-Wave Exposure: Theory Based on a Skin Model Coupled to a Whole Body Model and Local Biochemical Release From Cells at Supraphysiologic Temperatures

Donald A. Stewart, T. R. Gowrishankar, and James C. Weaver

***Abstract*—Energy dissipation by millimeter-wavelength electromagnetic-radiation (MMW; f $\sim$ 3 − 300 GHz) exposure to mammalian skin occurs within the outer surface. The penetration depth is less than 1 mm for frequencies above 25 GHz. A transport-lattice system model is used, which incorporates two spatial scales to estimate heat and chemical transport in rat skin *in vivo*: 1) a layered skin model involving the outer several millimeters of the body coupled to 2) a whole body model. The whole body model accounts for core-body heating, which provides a time-dependent reference temperature for blood perfusion in the skin model as well as the chemical concentration in the bloodstream and renal elimination. The model's thermal response to MMW exposure is consistent with the subcutaneous and colonic temperature measurements reported for 75 mW $\cdot$ cm^{-2} and 40-min exposures at 94 GHz in anesthetized rats. The simultaneous involvement of two biophysical mechanisms that create different chemical changes in response to the field exposure is also considered. First, a traditional nonspecific thermal-injury indicator is used to estimate denaturing molecular change due directly to heating as a function of depth in the skin. Rat skin exposed *in vivo* to 75 mW $\cdot$ cm^{-2} for long times (40 min) has a significant direct injury, while a 10-s exposure to 1 W $\cdot$ cm^{-2} results in a much less direct injury. Second, the biophysical mechanism of biochemical release through cell membranes within the tissue regions that reach supraphysiologic temperatures is also considered. The released molecules are delivered to other skin regions by diffusion and into the bloodstream by perfusion, where according to our hypothesis, the molecules interact with susceptible cells. This raises the possibility of additional indirect injury at nearby deeper skin regions that experience insignificant heating. Biochemical release may also lead to injury at distant sites within the body by perfusion clearance that transfers molecules into the systemic circulation to reach other susceptible cells. The hypothesis of simultaneous direct- and indirect-injury mechanisms is also illustrated by creating and solving didactic, coupled thermal, and chemical transport-lattice models.**

***Index Terms*—Chemical dose, microwaves, millimeter waves (MMWs), multiscale modeling, skin heating, skin injury, thermal mechanism, transport-lattice model.**

Manuscript received December 16, 2005; revised April 28, 2006. This work was supported in part by AFOSR Grant F49620-02-1-0372, in part by subcontract from Trinity University (manuscript approval number PA # 05-325), and in part by the National Institutes of Health under Grant GM63857.

The authors are with the Harvard-MIT Division of Health Sciences and Technology, Massachusetts Institute of Technology, Cambridge, MA 02139 USA (e-mail: jcw@mit.edu).

Digital Object Identifier 10.1109/TPS.2006.878996

I. Introduction

THE INTERACTION of electromagnetic fields with biological systems involves exposures ranging from continuous waves to short pulses and field magnitudes that range from "weak" to "strong" [1]. Electromagnetic waves in the frequency range 3–300 GHz are often referred to as millimeter waves (MMWs) and are of interest because of health and safety concerns [2]–[12] for diagnostic [13], [14] and therapeutic use [15], [16]. Both *in vivo* [17], [18] and *in vitro* [19], [20] studies have been carried out, and safety issues have been reviewed [21].

In the MMW region, heating is the only established mechanism for coupling electromagnetic fields to ongoing biochemical processes. Above $\sim$ 300 MHz, the tissue loses its electrical heterogeneity, and the important amplification mechanisms of voltage and current density concentration become small [22]. For this reason, we focus attention on the local electrical conductivity of skin tissue and estimate heating by considering the specific absorption rate (SAR) as a function of depth into the skin and then using the spatially varying SAR as a distributed input into a skin model for heat transport. Except for the outermost stratum corneum and epidermis, the skin tissue is well perfused [23], [24]. The resulting spatial and temporal temperature distributions $T(z,t)$ are used as input to the models that estimate injury interpretable as denaturing molecular change [25]–[27] and also biochemical release from the heated cells [28]–[30].

When the outer regions of the skin reach supraphysiologic temperatures, the cells can release molecules that then diffuse to the nearby skin layers and can also be transported to the rest of the body via blood perfusion. This raises the possibility of additional indirect injury at deeper skin regions. Biochemical release may also lead to injury at distant sites within the body by perfusion clearance that transfers the molecules into the systemic circulation. Fig. 1 illustrates the model. The idea is that some potent biochemical "s" is synthesized within the cells of the epidermis. Under normal conditions, the epidermal cell membrane has a low permeability to "s," which combined with systemic clearance maintains a concentration ($c_i \sim 1$ μM) within the source cells and a much lower concentration ($c \sim 10^{-3} c_i$) everywhere else. When the epidermis

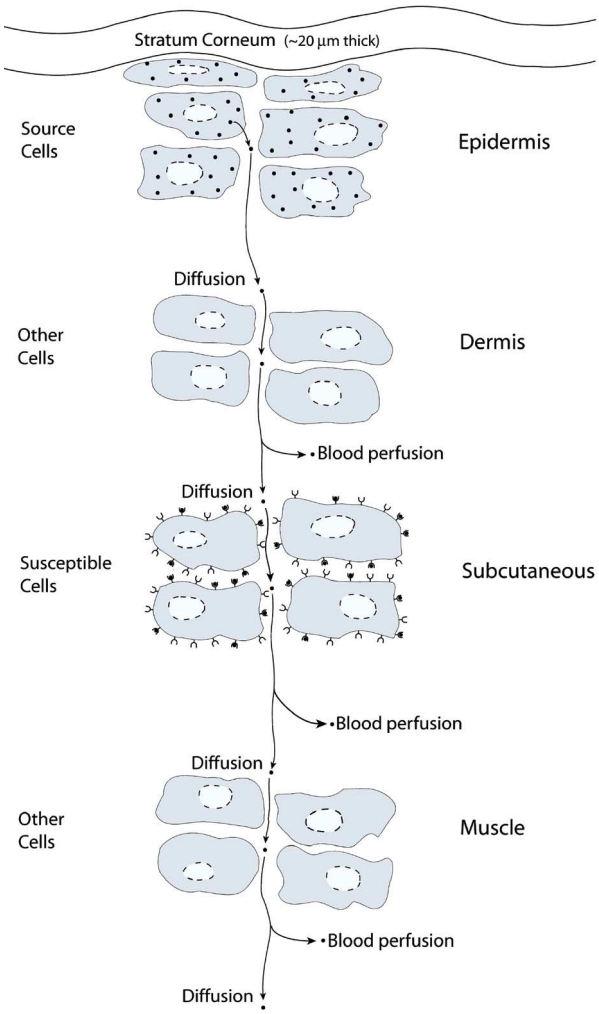

Fig. 1. Drawing illustrating a mechanism for indirect tissue injury by MMW skin heating. A hypothetical chemical species "s" is produced in epidermal cells near the skin surface. Under normal condition, the epidermal cell membrane has a low permeability that combined with systemic clearance maintains a high concentration within the source cells and a lower concentration everywhere else. When the epidermis undergoes heating, the membrane permeability to "s" increases, and the chemical concentration increases elsewhere through diffusion and perfusion. A layer of susceptible cells with receptors for "s" lies deep within the skin. The increased concentration of "s" in the susceptible layer can then result in observable injury to cells that would be indirectly due to the MMW exposure. (Color version available online at http://ieeexplore.ieee.org.)

undergoes heating, the membrane permeability to "s" increases, and the chemical concentration increases elsewhere through release, diffusion, and perfusion. An illustrative layer of cells with receptors for "s" is assumed to lie deep within the skin. The increased concentration of "s" in this susceptible layer can then result in indirect injury to deeper cells caused by MMW exposure through binding to the receptors specific to ligand "s."

A. In silico Electromagnetic-Field-Exposure Assessments

Previous examples of field-induced biochemical-change effects are accumulated transported ions through voltage-gated channels in a low-frequency periodic electric field applied to an isolated spherical cell [31] and elongated large cells [32], [33], dc electric-field net ion uptake changes in isolated cells [34], or the exquisite response of a shark to extraordinarily small ocean-

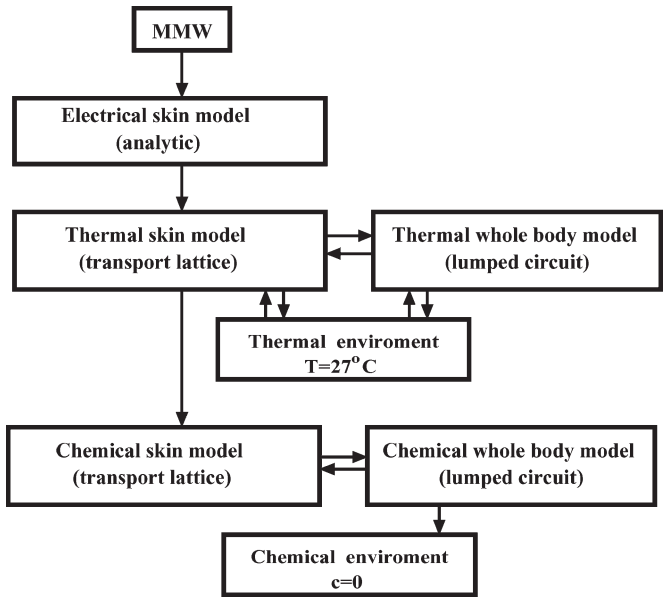

Fig. 2. Diagram showing relationships between elements of the system model. MMW radiation is incident on the outer layer of the skin. An analytical expression for the power absorbed as a function of depth provides the input for the transport-lattice thermal model of the skin. The thermal skin model is coupled to the thermal whole body model by thermal perfusion. The environment (27 °C) provides the reference temperature for the thermal model. As the outer layers of the skin are heated, the permeability of the epidermal cells increases, and chemical "s" is released into the extracellular space, where it diffuses to deeper layers and is taken simultaneously into the bloodstream by chemical perfusion.

water electric fields [35], and detection of small differences in the earth's magnetic field by magnetically sensitive chemical reactions [36]. Estimates of the molecular dose or field-induced chemical change are central to these estimates, which provide theoretical model-based initial assessments of a field exposure. If the field-induced molecular dose is comparable to chemical changes expected from other influences, then this approach can be used to estimate thresholds in the sense that a specific type of biophysical mechanism can be ruled out if the associated chemical-based signal-to-noise ratio is small or if the signal-to-noise ratio is relatively large that biophysical mechanism can be provisionally ruled in [37]. As models of biological systems with embedded biophysical mechanism are made more realistic, the results should provide a basis for *in silico* assessment of electromagnetic field exposures, which can guide the design and interpretation of experiments.

We illustrate the hypothesis of simultaneous direct- and indirect-injury mechanisms by creating and solving a system model with coupled thermal and chemical transport-lattice models. Fig. 2 outlines the thermal and chemical models. The power absorbed in the skin exposed to MMW radiation is calculated and then used as an input to the thermal lattice transport model. The core-body thermal model provides the reference temperature for thermal perfusion in the dermis, fat, and muscle layers. For an extended exposure, the core-body temperature itself rises. The local temperatures are then mapped into the chemical transport-lattice model to set the epidermal cell-membrane permeability. Chemical "s" is synthesized within the source epidermal cells at a constant rate and released into the interstitial space, transported within the interstitial space of

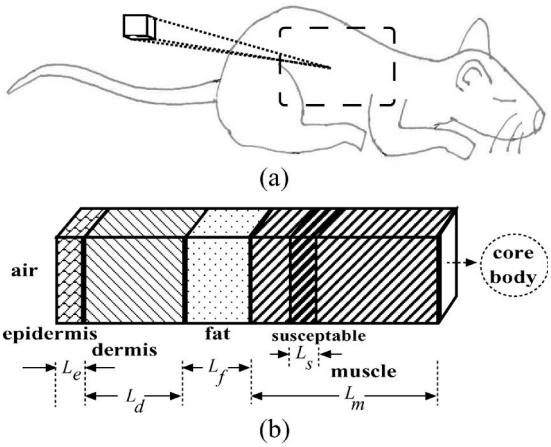

Fig. 3. Schematic showing region of exposure on the rat skin and an enlargement of the section of rat skin included in the transport-lattice model. (a) Exposure area is roughly 25% of the rat surface area. (b) Section of rat-skin geometry shows the rat skin with epidermal, dermal, subcutaneous fat, and muscle layers. Each of the four layers has different transport and storage properties. Thermal and chemical transport to and from the core is entirely via perfusion. The four-layer skin model has a cross-sectional area of $\Delta a = 0.01$ mm^2 and intranodal spacings of 0.8 μm ($= L_e/50$) for epidermis, 16 μm ($= L_d/50$) for dermis, 6 μm ($= L_f/50$) for subcutaneous adipose, and 200 μm ($= L_m/100$) for the muscle layer. The susceptible region is embedded within the muscle layer and is 800-μm thick.

the skin by diffusion, and into the bloodstream by perfusion. Chemical "s" is eventually accumulated in the bloodstream and then eliminated through the kidneys and bladder. Under normal conditions, a steady-state concentration profile of a few micromolar is established within the epidermal cells and subnanomolar everywhere else. The membrane permeability change in response to the MMW exposure leads to an increased concentration of "s" in the deeper tissue and in the bloodstream. The deeper tissue contains a layer of hypothetical receptor sites for "s," which makes this layer susceptible to injury from an increased concentration of "s."

II. Methods

A. Transport Lattice and Lumped Whole Body Models

The transport processes considered here (thermal and chemical) occur at two vastly different spatial scales. The smallest spatial scale is set by the characteristic penetration depth of 94-GHz MMW power absorbed in the skin, which is about 0.4 mm. An even smaller scale would be the membrane thickness ($\sim$ 5 nm), but membrane permeability to "s" is modeled by combining all the membranes of the cells within a local elemental volume of the lattice into a local lumped membrane permeability. The largest spatial scale is that of the entire animal ($\sim$ 10 cm) because the core-body temperature itself can change due to extensive exposure to MMW radiation. For the response in the skin, we use a transport-lattice model as described in a previous publication [26] with a lattice spacing much smaller than the characteristic penetration depth. For the whole body responses, we use lumped models with no spatial detail. The two extreme spatial scales are coupled by perfusion and systemic circulation. Fig. 3 shows the geometry of the layered skin tissue in the transport lattice. The geometry parameters for the rat and skin layers are given in Table I. The temperature (or concentration of "s") of the blood in the perfused tissue is set to be the core-body temperature (or concentration).

TABLE I
Geometry Parameters for the Rat and Layers of Skin

Δa	cross sectional area of skin model	$0.01\,\mathrm{mm}^2$	
Epidermis			
L_e	thickness	$40\,\mu$m	[38]
N_e	lattice elements	50	
ℓ_e	lattice node spacing	$0.8\,\mu$m	
ρ_e	density	1200 kg m^{-3}	[39]
Dermis			
L_d	thickness	$800\,\mu$m	[38]
N_d	lattice elements	50	
ℓ_d	lattice node spacing	$16\,\mu$m	
ρ_d	density	1060 kg m^{-3}	[39]
Subcutaneous Tissue			
t_f	thickness	$300\,\mu$m	
N_f	lattice elements	50	
ℓ_f	lattice node spacing	$6\,\mu$m	
ρ_f	density	1000 kg m^{-3}	[39]
Muscle Tissue			
t_m	thickness	20 mm	
N_m	lattice elements	100	
ℓ_m	lattice node spacing	$200\,\mu$m	
ρ_m	density	1040 kg m^{-3}	[39]
Blood			
V_b	blood volume	$34\,\mathrm{cm}^3$	[40]
ρ_b	density	1060 kg m^{-3}	[39]
Body			
M_{rat}	body mass	356 g	
V_{rat}	body volume	$343\,\mathrm{cm}^3$	
S_{rat}	body surface area	$236\,\mathrm{cm}^2$	
F_{exp}	fraction of surface exposed to MMW	0.25	
τ_b	blood circulation time constant	2 min	

B. MMW Power Absorption in Skin Tissue

The first step in solving the model is to calculate the power-absorption profile in the skin. This is accomplished by direct calculation of the power absorbed by Joule heating as a function of depth for 94-GHz MMW radiation. The calculation is based on the method described previously [26], [42], [43] except that, here, we allow for multiple internal reflections within the subcutaneous fat layer as well as in the dermis. Tissue parameters are given in Table II, and the calculated power-absorption profile versus depth is shown in Fig. 4. The power-absorption profile in Fig. 4 is given in units normalized to the power absorbed at the skin surface ($(P(x,t)/P(0,t))$, where the power absorbed $P(x,t)$ is in units of watts per cubic meter.

C. Heat Conduction and the Bioheat Equation for the Skin Model

Both heat conduction and perfusion occur simultaneously in a living tissue perfused by blood. As described by [26], we begin with local heat-conduction models and heat storage models and then add local models, which account for perfusion in the dermis, fat, and muscle layers (the stratum corneum and epidermis are not perfused [44]). All thermal model parameters are listed in Table III. The modular transport-lattice method employs interacting local models that describe local

TABLE II
ELECTRICAL-PROPERTY VALUES ASSIGNED TO DIFFERENT LAYERS OF SKIN

f_{MMW}	MMW frequency	94 GHz	
Air			
T_{sa}	air/skin transmission coefficient	0.69	
Epidermis/Dermis			
σ_e	conductivity	39.18 S m^{-1}	[41]
ϵ_e	relative permittivity	5.79	[41]
η_e	penetration depth	0.37 mm	[41]
λ_e	wavelength	1.16 mm	[41]
Subcutaneous Tissue			
σ_f	conductivity	3.47 S m^{-1}	[41]
ϵ_f	relative permittivity	2.91	[41]
η_f	penetration depth	2.6 mm	[41]
λ_f	wavelength	1.9 mm	[41]
Muscle Tissue			
σ_m	conductivity	61.5 S m^{-1}	[41]
ϵ_m	relative permittivity	9.02	[41]
η_m	penetration depth	0.30 mm	[41]
λ_m	wavelength	0.92 mm	[41]

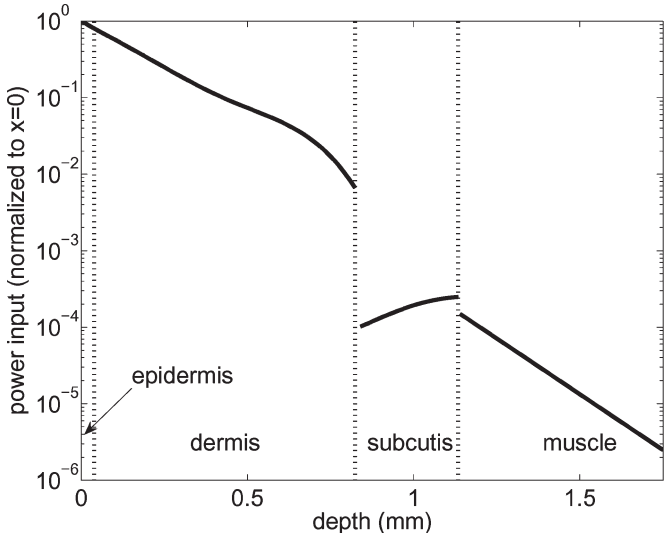

Fig. 4. Power absorbed in the skin tissue from incident 94-GHz MMW radiation. Result of analytical estimate of transmitted and reflected electric-field components of the EM wave. Each layer is assigned electrical conductivity and permittivities given by the Gabriel–Gabriel database for dielectric properties of tissue [41]. Changes in the dielectric properties result in the discontinuities. Multiple internal reflections within the dermal and fat layers result in the deviation of the profile from a simple exponential decay shape.

heat transport by conduction and by perfusion and local heat storage based on specific heat. The lattice of interconnected local models is then solved by applying Kirchhoff's laws to the equivalent circuit. To take advantage of the powerful robust circuit solving software (Berkeley SPICE 3f5), we use electrical circuits that are based on mathematical analogs to heat transport and storage. The transient circuit solution for voltages at each node corresponds to the temperature $T(x,t)$ as a function of depth x and time t for a given MMW exposure. The charge in the equivalent circuit is heat, and current corresponds to power. Fig. 5 shows the overall structure of the thermal transport lattice as well as the equivalent circuit elements. The chain of resistors between lattice nodes $(R_{\rm ce}, R_{\rm cd}, R_{\rm cf}, R_{\rm cm})$ and the capacitors connecting each node to ground $(C_{\rm ce}, C_{\rm cd}, C_{\rm cf}, C_{\rm cm})$ govern thermal conduction and heat capacitance in the local tissue element, while the resistors that connect each node to the core $(R_{\rm pd}, R_{\rm pf}, R_{\rm pm})$ govern thermal perfusion according to Penne's bioheat equation [26]. The current sources connected to each node $(I_{\rm ce}, I_{\rm cd}, I_{\rm cf}, I_{\rm cm})$ correspond to the MMW power dissipated in each local volume element of cross-sectional area Δa and lattice spacing ℓ. Thermal perfusion of the dermis, subcutis, and muscle layers corresponds to a resistive path to the core with a resistive element $R_{\rm pk}$. The transport-lattice elements for layer k, where k can be epidermis (e), dermis (d), subcutis (f), or muscle (m) are

$$\begin{aligned} R_{\rm ck} &= \frac{\ell_k}{k_k \Delta a} \\ C_{\rm ck} &= \rho_k c_k \ell_k \Delta a \\ I_{\rm ck} &= P(x,t) \Delta a \ell_k \\ R_{\rm pk} &= (\ell_k\ \Delta a\ \omega_k\ c_b\ \rho_b)^{-1} \end{aligned} \tag{1}$$

where the perfusion coefficient is ω_k, and the heat capacity and density of blood are c_b and ρ_b, respectively. The tissue density is ρ_k, the thermal conductivity is k_k, and the specific heat for tissue type k is c_k. At the left of the lattice, the resistance $R_{\rm ca}$ from the skin surface to the environment (air) corresponds to the heat-transfer coefficient of the skin surface

$$R_{\rm ca} = \frac{1}{g_a \Delta a}. \tag{2}$$

Table III lists the tissue properties referenced in (1) and (2). General aspects of methods used to construct, solve, and display the results of the transport-lattice system models are described elsewhere [24], [26], [45]. Here, we focus on spatially distributed skin heating caused by the 94-GHz MMW under the conditions used in the measurement described in [46].

The elements at the right end of the thermal transport lattice make up the thermal model for the core body and are discussed in the next section.

D. Core-Body Thermal Model

Description of the spatial and temporal temperature distribution $T(z,t)$ within the skin requires coupling to a core-body heating model because the net heat input into the body alters the core-body temperature and therefore the reference temperature in Penne's bioheat equation. For small animals under MMW exposures such as the anesthetized rats studied by Jauchem *et al.* [46], changes to the core-body temperature are significant. We use a simple model for core-body heating (Fig. 5) in which $C_{\rm c}$ represents the core-body heat capacity and $R_{\rm c}$ is a fixed thermal resistance that approximates all heat loss mechanisms (conduction, expired air, and gray body radiation) from the core body to the environment. We assume a constant basal metabolism ($I_{\rm c} = 0.1$ W), an initial core temperature of $T_{\rm c} = 37$ °C, and an environmental temperature maintained at $T_{\rm c} = 27$ °C. The core heat loss resistance $(R_{\rm c})$ is set by the

TABLE III
THERMAL-PROPERTY VALUES ASSIGNED TO DIFFERENT LAYERS OF SKIN

Air			
g_a	thermal surface conductivity coefficient	$6\ \mathrm{Wm^{-2}\,^{\circ}C^{-1}}$	
T_a	air temperature	27 °C	
Epidermis			
k_e	thermal conductivity	$0.23\ \mathrm{Wm^{-1}\,^{\circ}C^{-1}}$	[39]
c_e	specific heat	$3590\ \mathrm{J\ kg^{-1}\,^{\circ}C^{-1}}$	[39]
ω_e	perfusion rate	0	
Dermis			
k_d	thermal conductivity	$0.45\ \mathrm{Wm^{-1}\,^{\circ}C^{-1}}$	[39]
c_d	specific heat	$3300\ \mathrm{J\ kg^{-1}\,^{\circ}C^{-1}}$	[39]
ω_d	perfusion rate	$1.25\times10^{-3}\ \mathrm{m^3s^{-1}m^{-3}}$ tissue	[39]
Subcutaneous Tissue			
k_f	thermal conductivity	$0.19\ \mathrm{Wm^{-1}\,^{\circ}C^{-1}}$	[39]
c_f	specific heat	$2675\ \mathrm{J\ kg^{-1}\,^{\circ}C^{-1}}$	[39]
ω_f	perfusion rate	$1.25\times10^{-3}\ \mathrm{m^3s^{-1}m^{-3}}$ tissue	[39]
Muscle Tissue			
k_m	thermal conductivity	$0.5\ \mathrm{Wm^{-1}\,^{\circ}C^{-1}}$	[39]
c_m	specific heat	$3350\ \mathrm{J\ kg^{-1}\,^{\circ}C^{-1}}$	[39]
ω_m	perfusion rate	$1.56\times10^{-3}\ \mathrm{m^3s^{-1}m^{-3}}$ tissue	[39]
Blood			
c_b	specific heat	$3770\ \mathrm{J\ kg^{-1}\,^{\circ}C^{-1}}$	[39]
Body			
P_b	metabolic rate	0.1 W	
c_b	specific heat	$3350\ \mathrm{J\ kg^{-1}\,^{\circ}C^{-1}}$	[39]
T_c	Core temperature	37 °C	
Injury			
A_Ω	Ω attempt rate	$1.6\times10^{45}\ \mathrm{s^{-1}}$	[27]
E_Ω	Ω energy barrier	$5.1\times10^{-19}\mathrm{J\ molecule^{-1}}$	[27]

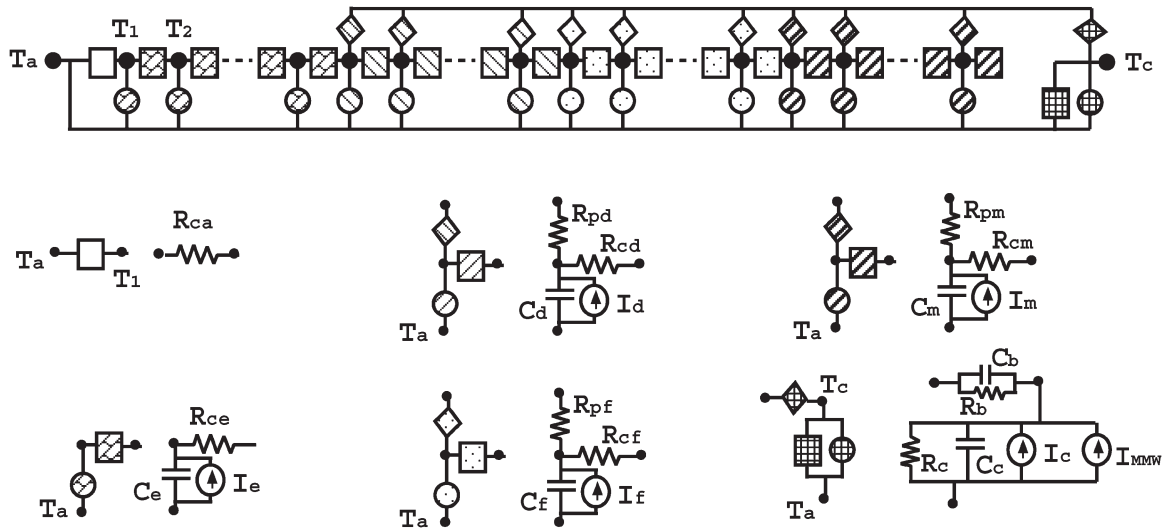

Fig. 5. Thermal transport-lattice model. The thermal model is represented by connections between various conductive local thermal models or elements (squares), storage elements (circles), and perfusion elements (diamonds). Each layer is identified by hatching pattern: Air (white), epidermis (bricks), dermis (angled), fat (dotted), muscle (angled), and core (cross hatched). The equivalent circuits for the various thermal elements are shown below the full circuit.

ratio of temperature difference and the metabolic rate, which is analogous to the ratio of electrical voltage and current

$$R_{\mathrm{c}} = (T_{\mathrm{c}} - T_{\mathrm{a}})/I_{\mathrm{c}} = 100\ ^{\circ}\mathrm{C/W}. \tag{3}$$

An additional heat current source (I_{MMW}) can be switched on that corresponds to the MMW power absorbed by the entire rat

$$I_{\mathrm{MMW}} = \left(\frac{F_{\mathrm{exp}} S_{\mathrm{rat}}}{\Delta a}\right) P(t - \tau_{\mathrm{b}}). \tag{4}$$

I_{MMW} is delayed from the incident MMW pulse by a characteristic time for blood circulation (τ_{b}). Here, F_{exp} is the fraction of the surface exposed to MMW pulse, and S_{rat} is the body surface area of the rat. The heat transported from the skin transport lattice to and from the core is also delayed by τ_{b} using an RC element.

E. Traditional Thermal-Injury Indicator Ω

Since introduced [25], thermal burns have often been analyzed by an Arrhenius rate constant equation that estimates the accumulation of some indicator of injury [47]–[49]. This

relationship was initially correlated with tissue injury, but can also be regarded as describing the transition of a native form of a hypothetical macromolecule to a denatured state. The Arrhenius rate constant expression provides a simple estimate based on a single injury process with Ω, which is a dimensionless indicator of accrued tissue injury [24], [47]. According to [48], the approximate injury threshold occurs at 42 °C. Below 42 °C, biological repair mechanisms prevent tissue injury. We estimate the accumulated injury [46] of the exposure as a function of x

$$\Omega(x) = A_\Omega \int_0^{t_{\exp}} e^{(-E_\Omega/kT(x,t'))} dt' \quad \Big|_{\text{for } t' \text{ with } T(x,t') \geq 42\ ^\circ\text{C}} \tag{5}$$

where $t_{\exp}$ is the length of the MMW exposure.

The values for A_Ω and E_Ω used in this paper are taken from [27] for the birefringence loss in the rat skin collagen and are listed in Table III. Pearce and Thomsen [27] did not use an injury-threshold temperature (42 °C) in their determinations of A_Ω and E_Ω, but we have included the injury threshold so that no injury is accrued for a null exposure. Complete epidermal necrosis corresponds to $\Omega \approx 1$.

F. Local Model For Chemical Release

The release of the hypothetical biochemical species "s" is a two-step process. First, the chemical is produced within the cells of the epidermis, and then it passes through the cell membrane into the interstitial fluid, where it diffuses to deeper layers and is taken up into the bloodstream. Eventually, the chemical is eliminated from the bloodstream via the kidneys. At steady state, the balance between production and elimination results in constant intracellular and extracellular concentrations. When exposed to MMW radiation, increased temperatures result in an increased extracellular and core-body concentration driven by the increased membrane permeability with temperature.

The model for the epidermal cell-membrane permeability to the illustrative biochemical "s" is based on experimental data for dipalmitoylphosphatidylcholine (DPPC) bilipid vesicle membrane permeability to glucose over a range of temperatures from 20 °C to 50 °C [28]. Details of the model for chemical transport and for membrane permeability are given in the appendices.

The flux of a chemical through the membrane ($J_{\rm s}$) is described by an Arrhenius rate model

$$\begin{aligned} J_{\rm s} &= P_{\rm s}(c_{{\rm s}i} - c_{{\rm s}o}) \\ &\approx v_{\rm rms} {\rm e}^{-E_{\rm s}/kT}(c_{{\rm s}i}) \end{aligned} \tag{6}$$

where $P_{\rm s}$ is the membrane permeability, $c_{{\rm s}i}$ and $c_{{\rm s}o}$ are the intracellular and extracellular concentrations of "s", respectively, $v_{\rm rms}$ is the mean thermal speed of "s" in the cell cytosol, and kT is the Boltzmann factor multiplied by the local temperature (in Kelvin). The energy barrier $E_{\rm s}$ is itself a function of temperature that undergoes a phase change at $T_L = 41.5$ °C

$$E_{\rm s} = E_{m0} + E_{m1}T - E_{m2}/\left(1 + e^{-(T-T_L)/\sigma_T}\right) \tag{7}$$

where E_{m0}, E_{m1}, E_{m2}, T_L, and σ_T are parameters described in Appendix I and listed in Table IV.

The expression for the number of "s" molecules crossing the epidermal cell membranes in a given elemental lattice volume is then

$$\frac{dn_{sm}}{dt} = 3\frac{v_{\rm rms}}{r_{\rm cell}}(\ell_e \Delta a f_{\rm v}) e^{-E_{\rm s}/kT}\,(c_{{\rm s}i} - c_{{\rm s}o}) \tag{8}$$

where $r_{\rm cell}$ is the characteristic length scale of the cells ($r_{\rm cell} = 10^{-5}$ m), ℓ_e is the epidermis lattice spacing, Δa is the skin-model cross-sectional area, and $f_{\rm v} = 0.85$ is the fractional volume taken up by the cells in the epidermis.

The production of the chemical within the epidermis cells is set to a constant rate, which results in a steady-state intracellular concentration of $c_{{\rm s}i} \sim 1$ μM and an extracellular concentration less than $c_{so} < 1$ nM. The rate of creation of "s" within the epidermal cells ($\dot{n}_{{\rm s}c}$) balances the flow of "s" through the membrane at normal epidermal temperatures $T_{\rm e} \sim 35$ °C. The creation rate of "s" can be estimated using (8) by setting $T = 37$ °C, $c_{{\rm s}i} = 1$ μM, and $c_{{\rm s}o} = 0$. The resulting "s" creation rate is $\dot{n}_{{\rm s}c}/(\ell_e \Delta a) = 10^{-11}$ μM/s in the epidermal cells. The parameter values are listed in Table IV.

G. Chemical Transport-Lattice Model

The released molecules "s" diffuse within the skin-tissue interstitial volume, partition into blood capillaries, and are swept into the systemic circulation by perfusion. The temperature dependence of the membrane permeability in (7) couples the chemical transport lattice (Fig. 6) to the heat transport lattice (Fig. 5). The structure of the chemical transport lattice is remarkably similar to the thermal lattice because of the underlying mathematical equivalence between the expressions for chemical and thermal diffusion and perfusion; the primary difference is in the values of the circuit elements and in the interpretation of the results. Appendix II gives a derivation for the basic expressions for the equivalent circuit elements for chemical diffusion in the chemical transport lattice. The geometry of the chemical transport lattice is the same as the thermal lattice so that the local temperature at a given node $T(x,t)$ provides input for the temperature-dependent membrane permeability.

Chemical transport-lattice elements for the skin layers are (where k is an index for the layers: epidermis e, dermis d, subcutis f, susceptible s, and muscle m)

$$\begin{aligned} R_{\rm sk} &= \frac{\ell_k}{D_{{\rm s}k} K_{{\rm s}k} \Delta a} \\ C_{\rm sk} &= K_{{\rm s}k} \ell_k \Delta a (1 - f_{\rm v}) \\ R_{\rm spk} &= (\ell_k\ \Delta a\ \omega_{sk})^{-1} \end{aligned} \tag{9}$$

where $D_{{\rm s}k}$ is the local diffusion coefficient for "s" in tissue k, $K_{{\rm s}k}$ is the local partition coefficient for "s" in tissue k, and ω_{sk} is the local perfusion coefficient for "s" in tissue k. Note that the chemical storage model $C_{\rm sk}$ is corrected for the fractional volume of the interstitial space $(1 - f_{\rm v})$. A corresponding correction for the tortuous diffusion pathways in the interstitial

TABLE IV
CHEMICAL "s" PROPERTY VALUES ASSIGNED TO DIFFERENT LAYERS OF SKIN

Epidermis			
D_{se}	diffusion coefficient	10^{-10} $\mathrm{m^2 s^{-1}}$	
K_{se}	partition coefficient	1	
ω_{se}	perfusion rate	0	
c_{sei}	initial intracellular concentration	1.6 μM	
v_{rms}	mean thermal speed of "s" within epidermal cells	170 $\mathrm{m\,s^{-1}}$	
r_{cell}	characteristic cell size	10 μm	
E_{m0}	membrane barrier coefficient	1.73×10^{-19} J molecule^{-1}	
E_{m1}	membrane barrier coefficient	-7.06×10^{-23} J molecule^{-1} K^{-1}	
E_{m2}	membrane barrier coefficient	-1.13×10^{-20} J molecule^{-1}	
T_m	membrane phase transition temperature	41.5 °C	
σ_T	membrane phase transition width	0.5 °C	
Dermis			
D_{sd}	diffusion coefficient	10^{-10} $\mathrm{m^2 s^{-1}}$	
K_{sd}	partition coefficient	1	
ω_{sd}	perfusion rate	0.63×10^{-3} $m^3 s^{-1} m^{-3}$ tissue	
Subcutaneous Tissue			
D_{sf}	diffusion coefficient	10^{-10} $\mathrm{m^2 s^{-1}}$	
K_{sf}	partition coefficient	1	
ω_{sf}	perfusion rate	0.63×10^{-3} $m^3 s^{-1} m^{-3}$ tissue	
Muscle Tissue			
D_{sm}	diffusion coefficient	10^{-10} $\mathrm{m^2 s^{-1}}$	
K_{sm}	partition coefficient	1	
ω_{sm}	perfusion rate	0.78×10^{-3} $\mathrm{m^3 s^{-1} m^{-3}}$ tissue	
t_{ss}	susceptible layer thickness	0.8 mm	
K_{ss}	susceptible layer partition coefficient	1.1	
Body			
r_u	rate of urine loss	0.23 $\mathrm{mm^3\,s^{-1}}$	[40]
F_{su}	filtration factor of "s"	10	

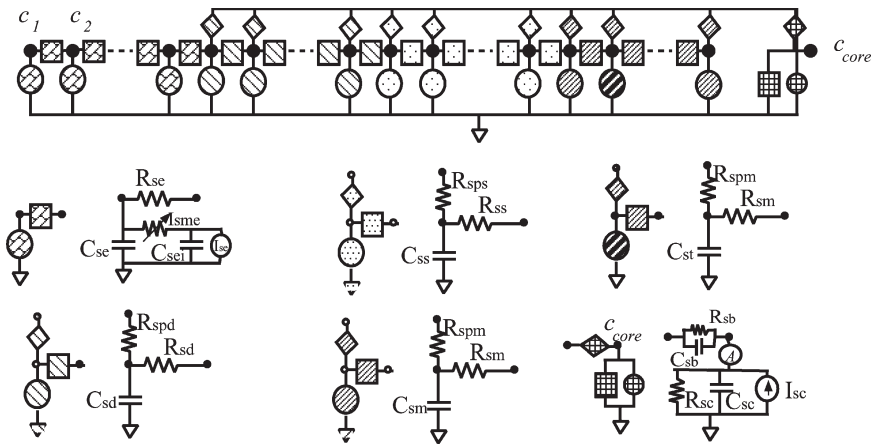

Fig. 6. Chemical transport-lattice model for a one-dimensional (1-D) rat-skin model and coupled whole body model. The diagram shows connections between various chemical diffusion elements (squares), storage elements (circles), and chemical perfusion elements (diamonds). Each layer is again identified by the hatching pattern: Air (white), epidermis (bricks), dermis (angled), fat (dotted), muscle (bold angled), susceptible (bold angled), and core (cross hatched). The equivalent circuits for the various chemical elements are shown below the full circuit. The chemical model is similar to the thermal model in Fig. 5. In most cases, the only difference is in the parameters, but there are more significant distinctions. For example, there is no path for the chemical to be released into the environment from the surface of the skin. All chemical release into the environment is done via the core-body model, which represents storage of the chemical in the blood stream and subsequent renal elimination. The chemical is synthesized (I_{sc}) within the epidermal cells at a steady rate. The epidermal cell-membrane permeability is temperature dependent and gives rise to a increased current (I_{sm}) of "s," as the local T increases due to MMW exposure. This explicit coupling between the thermal and chemical models provides a quantitative spatially distributed mechanism for the synthesis and transport of molecules within the skin model.

space for R_{sk} is included in the D_{sk} parameter. All chemical transport parameters are listed in Table IV.

Our model recognizes that the interstitial fluid represents about 15% of the human skin volume [44], [50], and we assume this value for the rat skin. Our model thus assumes that released molecules of type "s" dissolve into and diffuse within this extracellular compartment of the skin. Specifically, we use an effective volume that is $(1 - f_{\mathrm{v}}) = 0.15$ of the actual tissue volume of each of skin's layers. The diffusion coefficient in water is assumed to be $D_{\mathrm{s}} = 10^{-10}$ $\mathrm{m^2 \cdot s^{-1}}$ (independent of the local T). We use a temperature-independent diffusion coefficient D_{s} because the dominant temperature dependence is in the Boltzmann factor of (6). We also assume that the partition coefficient (relative solubility) for "s" between the interstitial fluid and blood is $K_{\mathrm{s}} = 1$, which is consistent with the effective clearance of small molecules from perfused tissue.

H. Chemical Susceptible Layer

To specifically illustrate our hypothesis, we assign an elevated partition coefficient ($K_{ss} = 1.1$) to the interstitial volume within a deep skin-tissue layer that has a negligible direct thermal injury (here $x = 1.3$ to 1.7 mm; Fig. 3). The assignment of a large K_{ss} mimics the binding of the released chemical species to the hypothetical binding sites at cells in this tissue region. The purpose of the present model is to explore the possibility that a potentially significant accumulation of thermally released molecules at deep skin regions is quantitatively plausible for some MMW exposures of interest.

The susceptible layer has a fixed number of ligand "s" receptor sites with a dissociation constant of

$$k_{\rm ds} = (c_{\rm s}c_{\rm b})/(c_{\rm bs}) \tag{10}$$

where the steady-state molar concentration of "s" is $c_{\rm s}$, the concentration of available receptor sites is $c_{\rm b}$, and the concentration of bound receptor sites is $c_{\rm bs}$. If we assume that the binding and unbinding rate is much faster than the changes in $c_{\rm s}$, then (10) is a constant even during transient changes in $c_{\rm s}$ at each local volume of the lattice. The total concentration of "s" in a given local volume is the sum of free "s" and bound "s," but only the free "s" can diffuse. The chemical potential of "s" depends on $c_{\rm s}$ but not directly on $c_{\rm bs}$. We also assume that the receptor sites are not close to saturation so that $c_{\rm b} \gg c_{\rm bs}$, making $c_{\rm b}$ a constant as well. Under these conditions, the chemical lattice equivalent circuit capacitance is

$$\begin{aligned} C_{ss} &= \Delta a \ell_s (1 - f_{\rm v})(1 + c_{\rm b}/k_{ds}) \\ &= \Delta a \ell_s (1 - f_{\rm v}) K_{ss} \end{aligned} \tag{11}$$

where the effective partition coefficient in the susceptible layer is $K_{ss} = (1 + c_{\rm b}/k_{ds})$. In our model, the partition coefficient in the susceptible layer is set to be 1.1, meaning that 10% of the total "s" contained in a local volume is always bound to a receptor.

I. Chemical Core-Body Model

The bloodstream acts as a chemical reservoir and serves as a path for renal elimination of chemical "s" from the body. These functions correspond to the $C_{\rm sc}$ capacitor and $R_{\rm sc}$ resistor in the chemical model schematic of Fig. 6. The volume that corresponds to the core volume is the volume of blood and interstitial fluid in the rat rather than the whole volume of the rat as was the case for the thermal heat capacitance. The renal elimination of "s" from the bloodstream is modeled on simple resistance. The value of resistance ($R_{\rm sc}$) is based on the basal urine production rate consistent with published rat data [40] and an assumption that the kidneys preferentially remove "s" from the bloodstream. The details of the model are described in Appendix II. The ratio of the steady-state concentrations in the urine to the bloodstream is assigned a value of $F_{\rm su} = 10$

$$\begin{aligned} R_{\rm sc} &= 1/(F_{\rm su} r_u) = 0.44 \text{ s} \cdot \text{mm}^{-3} \\ C_{\rm sc} &= V_b = 34 \times 10^3 \text{ mm}^3. \end{aligned} \tag{12}$$

The chemical influx to the core from the rest of the body is many orders of magnitude larger than the chemical from the skin transport-lattice model volume. This dominant component of the chemical influx is modeled using a current amplifier with an amplification factor of $F_{\rm exp} S_{\rm rat}/\Delta a$. The A component in the core model of the chemical lattice schematic shown in Fig. 6 is a SPICE ammeter (a 0-V voltage source) that measures the current from the small skin volume ($I_{\rm p}$) for use in the current source $I_{\rm c}$

$$I_{\rm c} = (F_{\rm exp} S_{\rm rat}/\Delta a) \times I_{\rm p}. \tag{13}$$

The current $I_{\rm p}$ is the rate of "s" from perfusion in the chemical transport lattice to the core. It is delayed by an RC ($= \tau_{\rm b}$) element before reaching the core. The resistance of the delay is set to be much smaller than the $R_{\rm spm}$ resistance so it does not significantly alter the steady-state concentration of "s." Thus, the local heat capacity is analogous to electrical capacitance, the local thermal resistance (reciprocal of thermal conductance) is analogous to electrical resistance, and the local specific absorption rate (SAR; power dissipation per tissue mass) is analogous to an electrical current source [26].

III. Results and Discussion

Transport-lattice system models that combined thermal and chemical local skin models and whole body models were constructed and simultaneously solved for two levels of 94-GHz MMW exposures. A "long" exposure based on the experimental methods of [46] used a 75 mW $\cdot$ cm^{-2} MMW intensity level for durations of 40 min. A "short" exposure has a 1-W $\cdot$ cm^{-2} MMW intensity for a duration of 10 s. The two exposures result in vastly different thermal (and chemical) responses.

A. Thermal-Response Distributions

The local temperature at each node of the skin transport lattice ($T(x,t)$) as well as the core-body temperature ($T_{\rm c}(t)$) is extracted from the SPICE solution for a given exposure level and is analyzed. Fig. 7 shows the temperature as a function of time at the skin surface (dashed), the subcutaneous fat layer (solid), and the core body (dot dash) for the "long" exposure [Fig. 7(a)] and the "short" exposure [Fig. 7(b)]. Superimposed on the "long" exposure model results are temperature measurements from [46], which show a reasonable agreement with the model for the thermal response to the 75 mW $\cdot$ cm^{-2} 40-min MMW exposure. The model shows a quicker initial response for the subcutis and a monotonic increase in the core temperature to the end of the exposure at 40 min. The data show a decrease in the core temperature after 30 min, which is probably due to physiological changes to the rat preceding death. No such change is included in the model, therefore there is no corresponding decrease in the core-body temperature leading up to 40 min. In the "long" exposure, the core body undergoes a significant increase in temperature to more than 41 °C, which is close to the onset of thermal injury [48].

The thermal response to "short" 10-s exposure is shown in Fig. 7(b). There is a sharp transient spike in temperature at

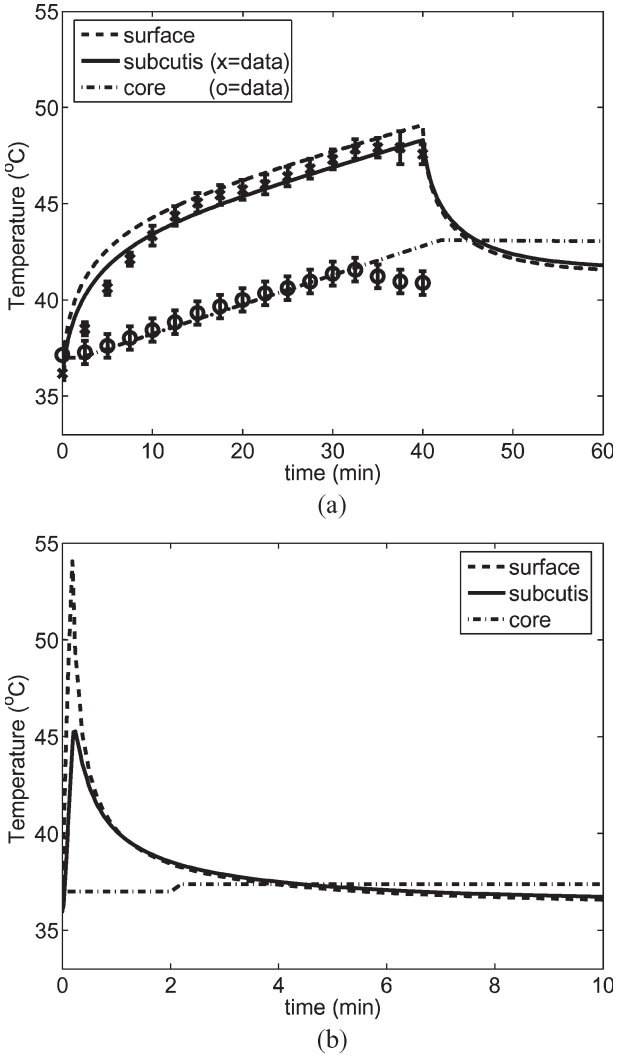

Fig. 7. Model for subcutaneous and colonic temperatures for an anesthetized rat exposed to **94** GHz. (a) Experimental data and model response for subcutaneous and colonic temperatures for an anesthetized rat exposed to 94 GHz at 75 mW $\cdot$ cm^{-2} for 40 min. The time-dependent temperatures reported by Jauchem *et al.* [46] can be explained by the transport-lattice model in Fig. 5. (b) Model response to MMW at 1 W $\cdot$ cm^{-2} for 10 s.

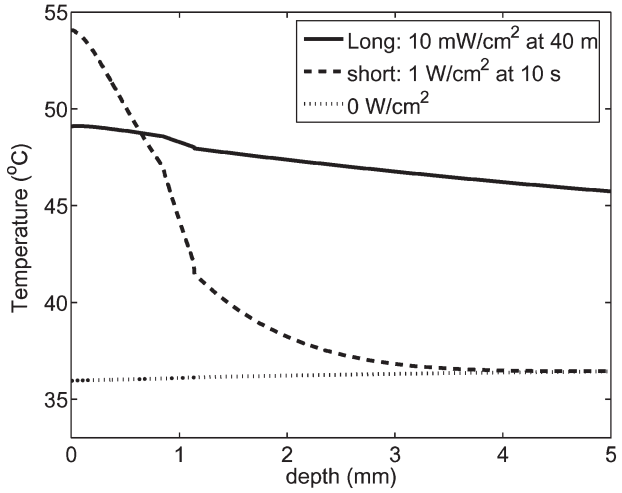

Fig. 8. Temperature depth profile resulting from exposure to 94-GHz MMW radiation. Temperature depth profiles $(T(x, t_{\exp}))$ at the end of the two MMW exposures (solid: 40 min, 75 mW $\cdot$ cm^{-2}; dashed: 10 s, 1 W $\cdot$ cm^{-2}) as well as the steady-state temperature profile for a null exposure (dotted). The "short" 10-s exposure results in a large temperature increase in the outer few millimeters of the skin but very little heating deeper than that. The "long" 40-min exposure heats the tissue far deeper into the skin, although the skin surface remains cooler than the "short" exposure (49 °C versus 54 °C).

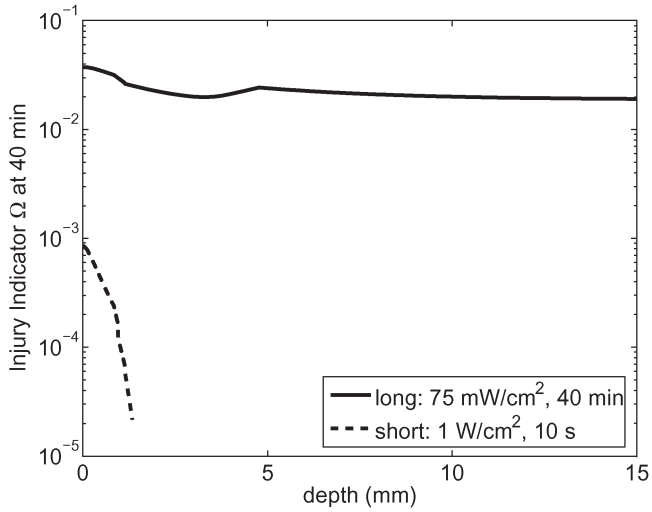

Fig. 9. Cumulative thermal-injury indicator **Ω**. Ω resulting from the "short" exposure (dashed) indicates negligible direct tissue injury, but for the "long" exposure, (solid) Ω indicates a significant accumulation of tissue injury by 40 min, although not at the severity of necrosis.

the surface to more than 50 °C, which is followed by a slow decrease. The surface temperature reaches 37 °C by 5 min. The subcutaneous layer has a transient spike to 45 °C and a decrease in temperature following the exposure. The core-body temperature is not significantly altered by the "short" MMW exposure.

Fig. 8 shows the calculated temperature versus the depth profiles $T(x, t_{\exp})$ at the time of the end of each exposure as well as the steady-state $T(x)$ for a null exposure. The "short" exposure (dashed) shows a large but short-lived temperature increase at 10 s in the outer few millimeters, which is in contrast to the "long" exposure (solid) penetrating far deeper into the animal by 40 min.

B. Thermal Injury

Direct thermal injury by MMW exposure based on the time-dependent temperature profile $T(x, t)$ is estimated using (5), and the accumulated injury at the time of the end of each exposure is plotted in Fig. 9. With the injury parameters listed in Table III, the accumulated injury from the "short" exposure is very small; however, the injury from the "long" exposure is larger and more extensive although still not reaching the point of necrosis.

C. Thermally Released Chemical-Concentration Response

The release of "s" from the epidermal cells is a consequence of MMW heating changing the cell-membrane permeability. The concentration of "s" in the interstitial space increases, and "s" diffuses to the nearby skin layers and perfuses into the bloodstream. Fig. 10 shows the concentration in the susceptible

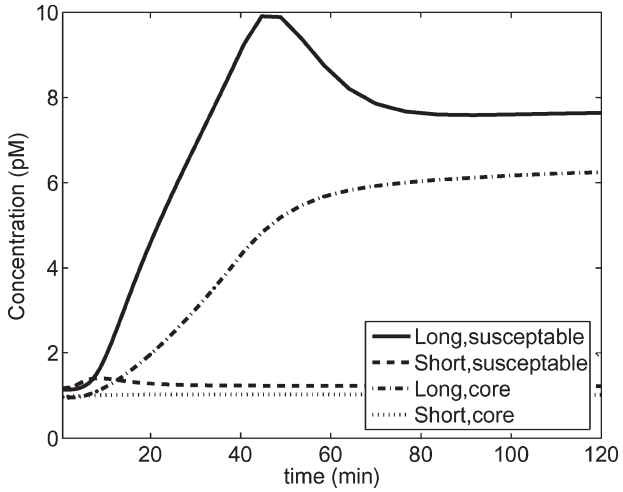

Fig. 10. Concentration of "s" in the susceptible region of the muscle layer and in the bloodstream for the two levels of MMW exposure. The concentration of "s" in the susceptible layer and the bloodstream rises by an order of magnitude in response to the "long" MMW exposure. In contrast, the "short" MMW exposure results in no significant change in the concentration of "s" at the susceptible region or in the bloodstream.

layer and in the core as a function of time for both "long" MMW exposure as well as the "short" exposure. For the "long" exposure, the susceptible and core concentrations rise from a level of about 1 pM to about 10 pM over the course of the 40-min-exposure duration and then slowly decay with a time constant governed by the renal elimination model ($C_{\rm sc}R_{\rm sc} \sim 4.2$ h). The "short" exposure results in a very little change in the concentration in either the susceptible layer or core body.

Fig. 11 shows the concentration of "s" as a function of depth into the skin at several times relative to the MMW pulse for both [Fig. 11(a)] "long" exposure and [Fig. 11(b)] "short" exposure.

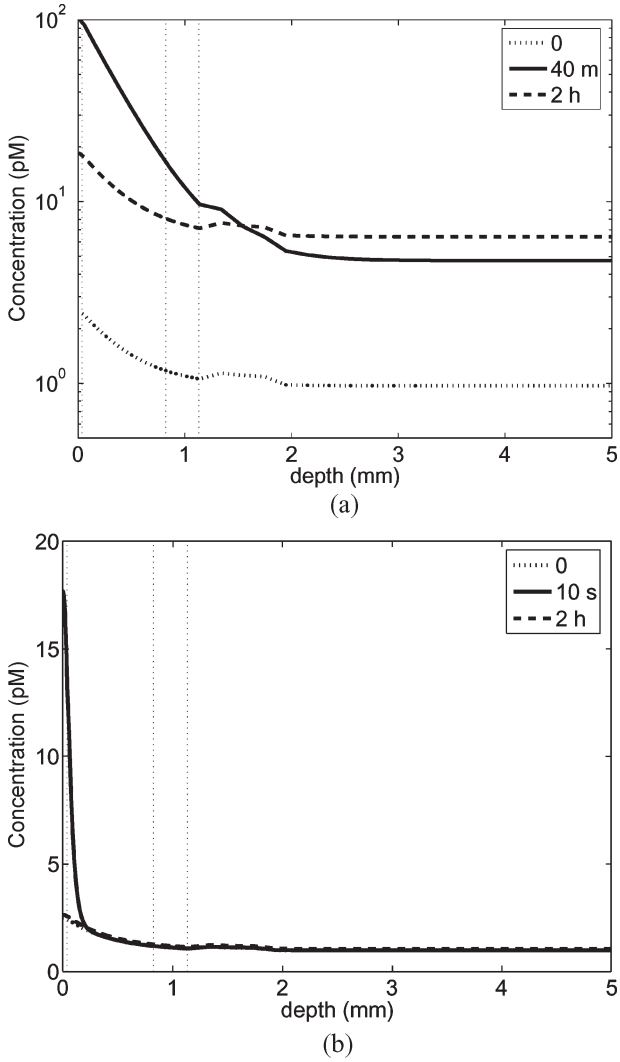

Fig. 11. Concentration depth profile $\mathbf{c_s}(\mathbf{x}, \mathbf{t})$ resulting from an exposure to 94-GHz MMW. (a) Long exposure at 75 mW $\cdot$ cm^{-2} at $t = 0$ (before exposure), $t = 40$ min (immediately after exposure), and $t = 2$ h (80 min after exposure). (b) Short exposure to 94-GHz MMW at 1 W $\cdot$ cm^{-2} for $t = 0$ (before exposure), $t = 10$ s, and $t = 2$ h (120 min after exposure). The two plots of effective concentration versus depth illustrate the hypothesis that release of water-soluble molecules "s" at local supraphysiological temperatures can be transported by tissue diffusion and perfusion to both nearby tissue sites and the systemic circulation, with the latter capable of targeting distant organs.

D. Relevance to Dermal Absorption and Transdermal Drug Delivery

Diffusive transport and perfusion clearance of biochemicals within the skin is relevant to unintended dermal absorption and to transdermal drug delivery.

The *in silico* predictions of the present models provide guidance for the design and analysis of future *in vivo* experiments. However, given the intrinsic complexity of electromagnetic field exposures and real tissues (variable, spatially varying physical, chemical, and biological features), progressively more complex modular models should be useful in understanding what is important to causing biological effects by electromagnetic fields, here MMW exposures of shaved skin of anesthetized rats.

E. Potential Experimental Tests

Samples of blood and plasma can be subjected to powerful genomics and proteomics analysis that search for fundamental changes at the molecular level in response to elevated temperatures at different tissue sites [51]. But the fact that blood communicates with essentially all of the body's organs and tissues means that association of changes with MMW heating of the skin is difficult. By quantitatively determining the nature of the chemical release and transport of biochemicals within the skin, the understanding of MMW injury and release of biomarkers should be significantly enhanced. Within the framework of this didactic model of chemical release, the locations, the sources and receptors, and properties of "s" can readily be changed to test hypotheses and compare with experiments.

A focus on molecular or chemical change due to a field exposure is relevant to understanding the conditions for which electromagnetic fields cause biological effects [37], [52]. Achieving sufficient field-induced molecular change relative to the changes in the same chemical species by competing influences is needed to interpret results from analysis such as proteomic profiling, which examines the response to "cold" (0 °C) or "hot" (45 °C) of skin-tissue cells removed from anesthetized mice [51].

APPENDIX I
MEMBRANE PERMEABILITY MODEL

A. Membrane-Permeability Temperature Dependence

The flux of molecules out of a cell through the plasma membrane is modeled by an Arrhenius rate expression

$$J_{\rm s} = A_{\rm s}(\Delta V/\Delta a)e^{-E_{\rm s}/kT}\left(c_{{\rm s}i} - c_{{\rm s}o}\right) = P_{\rm s}\left(c_{{\rm s}i} - c_{{\rm s}o}\right) \quad \text{(A1-1)}$$

where $A_{\rm s}$ is an attempt rate, ΔV is the cell volume, Δa is the membrane surface area, E_s is an energy barrier that can itself be a function of temperature, and $c_{{\rm s}i}$ and $c_{{\rm s}o}$ are the internal and external concentrations respectively. The membrane permeability $P_{\rm s}$ combines all these factors into a single temperature-dependent coefficient. We assume that the concentration within the cell $c_{{\rm s}i}$ is always much larger than the extracellular concentration $c_{{\rm s}o}$ so that $c_{{\rm s}o}$ in (A1-1) can be neglected. $A_{\rm s}$, $\Delta V/\Delta a$, and $E_{\rm s}$ parameters can be estimated, and the resulting permeability $P_{\rm s}$ is compared with data from the literature.

B. Attempt Rate

The attempt rate $A_{\rm s}$ is the expected rate that a given molecule within the cell will hit the membrane. We need only a rough estimate of the attempt rate $A_{\rm s}$ because the model is much more sensitive to the changes in $E_{\rm s}$ than $A_{\rm s}$. For estimation purposes, we assume a spherical cell of radius $r_{\rm cell}$. The mean free path of the molecule λ_s is much less than the cell radius. The mean speed of a pointlike molecule between collisions is $v_{\rm rms} = \sqrt{(2k_BT)/({\rm MW}u)}$, where MW is the molecular weight, and u is the atomic mass unit. Within an order of magnitude, the attempt rate depends on the speed, cell radius, and mean free path of the molecules within the cell

$$A_{\rm s} = \left(\frac{r_{\rm cell} - \lambda_{\rm s}}{r_{\rm cell}}\right)^3 \frac{v_{\rm rms}}{\lambda_{\rm s}} \approx 3\frac{v_{\rm rms}}{r_{\rm cell}}. \quad \text{(A1-2)}$$

The cubed term in (A1-2) is the probability that a given molecule will be within a λ_s of the membrane at $r_{\rm cell}$, and the $\lambda_s/v_{\rm rms}$ term is the expected time for such a molecule to hit the membrane. Substituting (A1-2) into (A1-1) and noting that $\Delta V/\Delta a = r_{\rm cell}/3$ for a spherical cell, we can simplify (A1-1)

$$J_{\rm s} = v_{\rm rms}e^{-E_{\rm s}/kT}c_{{\rm s}i}$$

and the permeability coefficient

$$P_{\rm s} = v_{\rm rms}e^{-E_{\rm s}/kT}. \quad \text{(A1-3)}$$

C. Energy-Barrier Temperature Dependence from Permeability Data

Given the data from [28] for the permeability of glucose through the bilayer membranes, we can estimate the energy-barrier dependence on temperature. Fig. 12 shows a comparison between the data for DPPC lipid bilayer membranes and the model based on (A1-3). The expression for the energy barrier $E_{\rm s}$ is

$$E_{\rm s} = E_0 + E_1T - E_3/\left(1 + e^{-(T-41.5\ ^\circ{\rm C})/(0.5\ ^\circ{\rm C})}\right) \quad \text{(A1-4)}$$

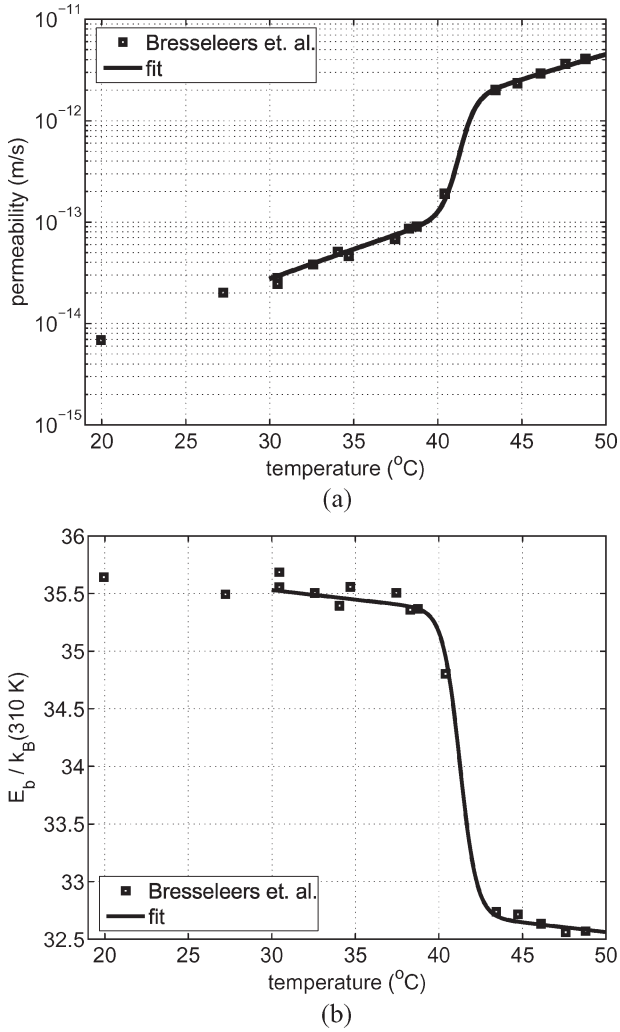

Fig. 12. Membrane permeability model. Data for glucose permeability through DPPC lipid bilayer membranes compared to Arrhenius rate model of (A1-3). (a) Permeability $P_{\rm s}$ versus T. (b) Energy barrier $E_{\rm s}$ versus T.

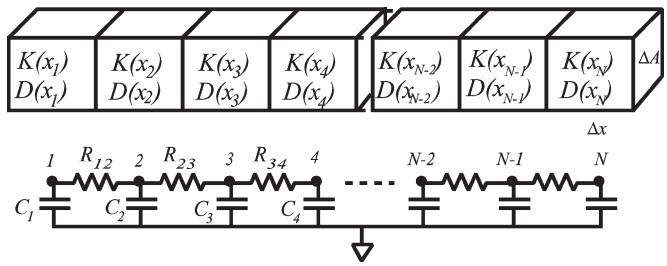

Fig. 13. Schematic of equivalent circuit for 1-D diffusion: 1-D chemical diffusion lattice transport model with varying diffusion and partition coefficients and the equivalent circuit representation.

which is a linear dependent E_s with a sigmoid jump at $T = 41.5\ ^\circ$C. The fitted parameters are $E_0 = 104.4$ kJ $\cdot$ mole^{-1}, $E_1 = -0.0424$ kJ $\cdot$ mole$^{-1} \cdot$ K^{-1}, and $E_3 = 6.8$ kJ/mole. In [28], the "activation" energy is described as a constant rather than a linear function of T away from the critical temperature, but our model allows for a linear component.

APPENDIX II
CHEMICAL TRANSPORT LATTICE

A. Homogeneous Volume

We derive an equivalent circuit for the chemical diffusion in one dimension of chemical species in a homogeneous volume of cross-sectional area ΔA and depth L (Fig. 13) . In the homogeneous case, the diffusion coefficient, partition coefficient, and temperature are constant throughout the volume. The chemical flux J_s is driven by the gradient of the concentration c_s according to Fick's law for dilute solutions

$$J_s = -D_s \nabla c_s \tag{A2-1}$$

where D_s is the diffusion coefficient for solute "s". This is mathematically equivalent to the expression for electrical current density

$$J = -\sigma \nabla v \tag{A2-2}$$

with the identification of the conductivity σ with the diffusion coefficient D_s, voltage v with concentration, and current density with chemical flux.

B. Boundary Between Volumes of Different D_s and K_s

At a boundary between volumes with different diffusion coefficients (D_{s1} and D_{s2}) and a partition coefficient ($K_s = c_{s2}/c_{s1}$ at equilibrium), the boundary conditions are

1) continuity of normal flux ($J_{s1} = J_{s2}$);
2) continuity of chemical potential ($\mu_{s1} = \mu_{s2}$).

The boundary is located midway between two elemental volumes with nodes at the centers. The flux condition is satisfied since there are no alternate current paths at the boundary. The chemical potential μ_s can be expressed in terms of a constant for the given solute and solution $\mu_{s,0}$ and the concentration of the solute c_s

$$\mu_s = \mu_{s,0} + k_B T \ln\left(\frac{a_s c_s}{\sum_i c_i}\right) \tag{A2-3}$$

where k_B is Boltzmann's constant, T is the local temperature, a_s is an activity coefficient, and the sum is the over all concentrations of molecule types in the solution. The continuity of chemical potential across the boundary corresponds to a jump in the μ_{s0} term

$$\begin{aligned}\Delta\mu_{s0} &= -k_B T \ln(c_{s2b}/c_{s1b}) \\ &= -k_B T \ln(K_s)\end{aligned} \tag{A2-4}$$

where K_s is defined as the partition coefficient of the solute "s" in medium 2 relative to medium 1. This expression for $\Delta\mu_{s0}$ assumes a uniform T, and that a_s and $\sum_i c_i$ are same on either side of the boundary. The concentrations at nodes 1 and 2 are c_{s1} and c_{s2}, respectively. At the boundary, the concentration jumps from c_{s1b} on the left to $c_{s2b} = K_s c_{s1b}$ on the right. The flux going into the boundary from side 1 is J_{s1}, and the flux from the boundary on side 2 is J_{s2}. The elemental expressions for J_{s1} and J_{s2} from Fick's law are

$$\begin{aligned}J_{s1} &= -\frac{2D_{s1}}{\Delta x}(c_{s1b} - c_{s1}) \\ J_{s2} &= -\frac{2D_{s2}}{\Delta x}(c_{s2} - c_{s2b}) \\ &= -\frac{2D_{s2}K_s}{\Delta x}(c_{s2}/K_s - c_{s1b}).\end{aligned} \tag{A2-5}$$

On side 2, there is an extra factor of K_s that changes the electrical equivalence such that the concentration must be divided by the partition coefficient to be identified with voltage. The conductivity is identified with the diffusion coefficient multiplied by the partition coefficient.

C. Diffusion in 1-D With Spatially Varying $D_s(x)$ and $K_s(x)$

The equivalent circuit from the boundary is extended to volumes with varying diffusion coefficients as well as variable partitioning, continuous or discontinuous, with the convention of defining a partition coefficient as a function of x, $K_s(x)$, as the ratio of equilibrium concentrations relative to a single location, say $x = 0$. The chemical potential expression from (A2-3) assumes the form

$$\begin{aligned}\mu_s(x) &= \mu_{s0} - k_B T\left(\ln\left(\frac{a_s c_s(x)}{\sum_i c_i}\right) - \ln\left(K_s(x)\right)\right) \\ &= \mu_{s0} - k_B T\left(\ln\left(\frac{a_s c_s(x)}{K_s(x)\sum_i c_i}\right)\right).\end{aligned} \tag{A2-6}$$

The generalized expression for chemical flux is based on the gradient of the chemical potential

$$J_s = -\frac{D_s c_s}{k_B T}\nabla\mu_s \tag{A2-7}$$

which reduces to (A2-1) when D_s, K_s, a_s, and T are constant, but becomes

$$J_s(x) = -D_s(x)K(x)\nabla\left(\frac{c_s(x)}{K_s(x)}\right) \tag{A2-8}$$

when D_s and K_s depend on the position. This expression has the same form as (A2-2) with the identification of the electrical conductivity σ with $D_s(x)K_s(x)$ and the voltage V with $(c_s(t,x)/K_s(x))$. Table V lists the generalized equivalent circuit elements.

We note that in the gradient of the chemical potential in (A2-8), there is a term with the gradient of T, which is assumed to be negligible. In the thermal model described in this paper,

TABLE V
CHEMICAL DIFFUSION PARAMETERS AND ELECTRICAL EQUIVALENTS CORRESPONDING TO FIG. 13

Chemical Diffusion	Equivalent Circuit	
$c_{\rm s}(t,x)/K_{\rm s}(x)$	$V(t,x)$	concentration and voltage
$D(x)\cdot K_{\rm s}(x)$	$\sigma(x)$	diffusion, partition coefficient and conductance
$K_{\rm s}(x)\cdot\Delta a\Delta x$	$C(x)$	partition coefficient and capacitance
$\frac{\Delta x}{\Delta a D_{\rm s}(x)K_{\rm s}(x)}$	$R(x)$	resistance between nodes

T is not a constant, however, $\nabla T/T$ is more than 1000 times smaller than $\nabla\ln(c_{\rm s})/\ln(c_{\rm s})$ in all conditions modeled in this paper, so the contribution of the temperature gradient to the chemical flux is negligible.

ACKNOWLEDGMENT

The authors would like to thank R. Sypniewski, N. Millenbaugh, G. T. Martin, P. A. Mason, R. V. Blystone, and E. R. Adair for the important discussions. They would also like to thank K. G. Weaver for the graphics and computer support.

REFERENCES

[1] C. Polk and E. Postow, Eds., *CRC Handbook of Biological Effects of Electromagnetic Fields*, 2nd ed. Boca Raton, FL: CRC Press, 1996.
[2] E. P. Khizhnyak and M. C. Ziskin, "Heating patterns in biological tissue phantoms caused by millimeter wave electromagnetic irradiation," *IEEE Trans. Biomed. Eng.*, vol. 41, no. 9, pp. 865–873, Sep. 1994.
[3] M. R. Frei, K. L. Ryan, R. E. Berger, and J. R. Jauchem, "Sustained 35-GHz radiofrequency irradiation induces circulatory failure," *Shock*, vol. 4, no. 4, pp. 289–293, Oct. 1995.
[4] P. J. Riu, K. R. Foster, D. W. Blick, and E. R. Adair, "A thermal model for human thresholds of microwave-evoked warmth sensations," *Bioelectromagnetics*, vol. 18, no. 8, pp. 578–583, 1997.
[5] D. W. Blick, E. R. Adair, W. D. Hurt, C. J. Sherry, T. J. Walters, and J. H. Merritt, "Thresholds of microwave-evoked warmth sensations in human skin," *Bioelectromagnetics*, vol. 18, no. 6, pp. 403–409, 1997.
[6] A. G. Pakhomov, Y. Akyel, O. N. Pakhomova, B. E. Stuck, and M. R. Murphy, "Current state and implications of research on biological effects of millimeter waves: A review of the literature," *Bioelectromagnetics*, vol. 19, no. 7, pp. 393–413, 1998.
[7] K. R. Foster and L. S. Erdreich, "Thermal models for microwave hazards and their role in standards development," *Bioelectromagnetics*, vol. 4, Suppl. 4, pp. 52–63, 1999.
[8] T. J. Walters, D. W. Blick, L. R. Johnson, E. R. Adair, and K. R. Foster, "Heating and pain sensation produced in human skin by millimeter waves: Comparison to a simple thermal model," *Health Phys.*, vol. 78, no. 3, pp. 259–267, Mar. 2000.
[9] D. A. Nelson, T. J. Walters, K. L. Ryan, K. B. Emerton, W. D. Hurt, J. M. Ziriax, L. R. Johnson, and P. A. Mason, "Inter-species extrapolation of skin heating resulting from millimeter wave irradiation: Modeling and experimental result," *Health Phys.*, vol. 84, no. 5, pp. 608–615, May 2003.
[10] K. R. Foster, J. A. D'Andrea, S. Chalfin, and D. J. Hatcher, "Thermal modeling of millimeter wave damage to the primate cornea at 35 GHz and 95 GHz," *Health Phys.*, vol. 84, no. 6, pp. 764–769, Jun. 2003.
[11] T. J. Walters, K. L. Ryan, D. A. Nelson, D. W. Blick, and P. A. Mason, "Effects of blood flow on skin heating induced by millimeter wave irradiation in humans," *Health Phys.*, vol. 86, no. 2, pp. 115–120, Feb. 2004.
[12] K. R. Foster and E. R. Adair, "Modeling thermal responses in human subjects following extended exposures to radiofrequency energy," *Biomed. Eng. Online*, vol. 3, no. 1, p. 4, 2004.
[13] R. K. Cacak, D. E. Winans, J. Edrich, and W. R. Hendee, "Millimeter wavelength thermographic scanner," *Med. Phys.*, vol. 8, no. 4, pp. 462–465, Jul./Aug. 1981.
[14] J. Edrich and C. J. Smyth, "Arthritis inflammation monitored by subcutaneous millimeter wave thermography," *J. Rheumatol.*, vol. 5, no. 1, pp. 59–67, 1978.
[15] A. A. Radzievsky, M. A. Rojavin, A. Cowan, and M. C. Ziskin, "Suppression pain sensation caused by millimeter waves: A double-blinded, cross-over, prospective human volunteer study," *Anesth. Analg.*, vol. 88, no. 4, pp. 836–840, Apr. 1999.
[16] N. F. Miryutova, E. F. Levitskii, A. M. Kozhemyakin, and I. M. Mavlyautdinova, "Millimeter waves in the treatment of neurological manifestations of vertebral osteochondrosis," *Crit. Rev. Biomed. Eng.*, vol. 29, no. 5/6, pp. 613–621, 2001.
[17] A. A. Radzievsky, A. Cowan, C. Byrd, A. A. Radzievsky, and M. C. Ziskin, "Single millimeter wave treatment does not impair gastrointestinal transit time in mice," *Life Sci.*, vol. 71, no. 15, pp. 1763–1770, Aug. 2002.
[18] M. K. Logani, A. Anga, I. Szabo, A. Agelan, A. R. Irizarry, and M. C. Ziskin, "Effects of millimeter waves on cyclophosphamide induced suppresion of the immune system," *Bioelectromagnetics*, vol. 23, no. 8, pp. 614–621, Dec. 2002.
[19] L. J. Stensaas, L. M. Partlow, L. G. Bush, P. L. Iversen, D. W. Hill, M. J. Hagmann, and O. P. Gandhi, "Effects of millimeter-wave radiation on monolayer cell cultures. II. Scanning and transmission electron microscopy," *Bioelectromagnetics*, vol. 2, no. 2, pp. 141–150, 1981.
[20] I. Szabo, M. A. Rojavin, T. J. Rogers, and M. C. Ziskin, "Reactions of keratinocytes to in vitro millimeter wave exposure," *Bioelectromagnetics*, vol. 22, no. 5, pp. 358–364, Jul. 2001.
[21] K. L. Ryan, J. A. D'Andrea, J. R. Jauchem, and P. A. Mason, "Radio frequency radiation of millimeter wave length: Potential occupational safety issues relating to surface heating," *Health Phys.*, vol. 78, no. 2, pp. 170–181, Feb. 2000.
[22] T. R. Gowrishankar and J. C. Weaver, "An approach to electrical modeling of single and multiple cells," *Proc. Nat. Acad. Sci.*, vol. 100, no. 6, pp. 3203–3208, Mar. 2003.
[23] C. W. Song, "Effect of local hyperthermia on blood flow and microenvironment: A review," *Cancer Res.*, vol. 44, no. 10, pp. 4721S–4730S, Oct. 1984.
[24] T. Nagaska, K. Hirata, T. Nunomura, and M. Cabanac, "The effect of local heating on blood flow in the finger and the forearm skin," *Can. J. Physiol. Pharmacol.*, vol. 65, no. 6, pp. 1329–1332, Jun. 1987.
[25] A. R. Moritz and F. C. Henriques, "Studies of thermal injury. II. The relative importance of time and surface temperature in the causation of cutaneous burns," *Amer. J. Pathol.*, vol. 26, pp. 695–720, 1947.
[26] T. R. Gowrishankar, D. A. Stewart, G. T. Martin, and J. C. Weaver, "Transport lattice models of heat transport in skin with spatially heterogeneous, temperature-dependent perfusion," *Biomed. Eng. Online*, vol. 3, no. 1, p. 42, Nov. 2004.
[27] J. A. Pearce and S. Thomsen, "Kinetic models of laser-tissue fusion processes," *Biomed. Sci. Instrum.*, vol. 29, pp. 355–360, 1993.
[28] G. J. M. Bresseleers, H. L. Goderis, and P. P. Tobback, "Measurement of the glucose permeation rate across phospholipid bilayers using small unilamellar vesicles: Effect of membrane composition and temperature," *Biochim. Biophys. Acta*, vol. 772, no. 3, pp. 374–382, May 1984.
[29] G. Cevec and D. Marsh, *Phospholipid Bilayers*. New York: Wiley, 1987.
[30] S. Bhowmick, D. J. Swanlund, and J. C. Bishof, "Supraphysiological thermal injury in Dunning AT-1 prostate tumor cells," *J. Biomech. Eng.*, vol. 122, no. 1, pp. 51–59, Feb. 2000.
[31] R. D. Astumian, J. C. Weaver, and R. K. Adair, "Rectification and signal averaging of weak electric fields by biological cells," *Proc. Nat. Acad. Sci.*, vol. 92, no. 9, pp. 3740–3743, Apr. 1995.
[32] J. C. Weaver, T. E. Vaughan, R. K. Adair, and R. D. Astumian, "Theoretical limits on the threshold for the response of long cells to weak ELF electric fields due to ionic and molecular flux rectification," *Biophys. J.*, vol. 75, no. 5, pp. 2251–2254, Nov. 1998.
[33] J. C. Weaver, T. E. Vaughan, and G. T. Martin, "Biological effects due to weak electric and magnetic fields: The temperature variation threshold," *Biophys. J.*, vol. 76, no. 6, pp. 3026–3030, Jun. 1999.
[34] P. C. Gailey, "Membrane potential and time required for detection of weak signals by voltage-gated ion channels," *Bioelectromagnetics*, vol. 20, Suppl. 4, pp. 102–109, 1999.
[35] R. K. Adair, R. D. Astumian, and J. C. Weaver, "On the detection of weak electric fields by sharks, rays and skates," *Chaos*, vol. 8, no. 3, pp. 576–587, Sep. 1998.
[36] J. C. Weaver, T. E. Vaughan, and R. D. Astumian, "Magnetically sensitive chemical reactions can provide biological sensing of small field differences," *Nature*, vol. 405, pp. 707–709, Jun. 8, 2000.
[37] T. E. Vaughan and J. C. Weaver, "Molecular change signal-to-noise criteria for interpreting experiments involving exposure of biological systems to weakly interacting electromagnetic fields," *Bioelectromagnetics*, vol. 26, no. 4, pp. 305–322, May 2005.

[38] T. Ngawhirunpat, T. Hatanaka, K. Katayama, H. Yoshikawa, J. Kawakami, and I. Adachi, "Changes in electrophysiological properties of rat skin with age," *Biol. Pharm. Bull.*, vol. 25, no. 9, pp. 1192–1196, Sep. 2002.
[39] D. A. Torvi and J. D. Dale, "A finite element model of skin subjected to a flash fire," *ASME J. Biomech. Eng.*, vol. 116, no. 3, pp. 250–255, Aug. 1994.
[40] P. Sharp and M. LeRegina, *The Laboratory Rat*. New York: CRC Press, 1998.
[41] C. Gabriel and S. Gabriel, "Compilation of the dielectric properties of body tissues at RF and microwave frequencies," Kings College, London, U.K., Tech. Rep. AL/OE-TR-1996-0037, 1996. [Online]. Available: http://www.brooks.af.mil/AFRL/HED/hedr/reports/dielectric/Report/Report.html
[42] A. Balanis, *Advanced Engineering Electromagnetics*. New York: Wiley, 1989.
[43] F. Gustrau and A. Bahr, "W-band investigation of material parameters, SAR distribution, and thermal response in human tissue," *IEEE Trans. Microw. Theory Tech.*, vol. 50, no. 10, pp. 2393–2400, Oct. 2002.
[44] H. Schaefer and T. E. Redelmeier, *Skin Barrier: Principles of Percutaneous Absorption*. Basel, Switzerland: Karger, 1996.
[45] D. A. Stewart, T. R. Gowrishankar, and J. C. Weaver, "Transport lattice approach to describing cell electroporation: Use of a local asymptotic model," *IEEE Trans. Plasma Sci.*, vol. 32, no. 4, pp. 1696–1708, Aug. 2004.
[46] J. R. Jauchem, K. L. Ryan, and M. R. Frei, "Cardiovascular and thermal responses in rats during 94 GHz irradiation," *Bioelectromagnetics*, vol. 20, no. 4, pp. 264–267, 1999.
[47] K. R. Diller, "The mechanisms and kinetics of heat injury accumulation," in *Electrical Injury: A Multidisciplinary Approach to Therapy, Prevention*, vol. 72, R. C. Lee, M. Capelli-Schellpfeffer, and K. M. Kelly, Eds. New York: N.Y. Acad. Sci, 1994, pp. 38–55.
[48] R. C. Lee, G. Russo, and G. Kicska, "Kinetics of heating in electrical shock," in *Electrical Injury: A Multidisciplinary Approach to Therapy, Prevention*, vol. 720, R. C. Lee, M. Capelli-Schellpfeffer, and K. M. Kelly, Eds. New York: N.Y. Acad. Sci, 1994, pp. 56–64.
[49] E. Y.-K. Ng and L. T. Chua, "Prediction of skin burn injury. Part 2: Parametric and sensitivity analysis," *Proc. Inst. Mech. Eng.*, vol. 216, pt. H, pp. 171–183, 2002.
[50] K. Halprin, A. Ohkawara, and K. Adachi, "Glucose entry into the human epidermis. I. The concentration of glucose in the human epidermis," *J. Invest. Dermatol.*, vol. 49, no. 6, pp. 559–560, Dec. 1967.
[51] C. Huang, K. Foster, T. DeSilva, J. Zhang, Z. Shi, N. Yusuf, K. V. Kampen, C. Elmets, and D. Tang, "Comparative proteomic profiling of murine skin," *J. Invest. Dermatol.*, vol. 121, no. 1, pp. 51–64, Jul. 2003. [Online]. Available: http://www.blackwell-synergy.com/doi/abs/10.1046/j.1523-1747.2003.12327.x
[52] J. C. Weaver, "Understanding conditions for which biological effects of nonionizing electromagnetic fields can be expected," *Bioelectrochemistry*, vol. 56, no. 1/2, pp. 207–209, May 2002.

Donald A. Stewart received the B.S. degree from the University of Illinois, Champaign, in 1981 and the Ph.D. degree in high-energy physics from Indiana University, Bloomington, in 1988.

He did postdoctoral work at the Ferni National Accelerator Laboratory, Batavia, IL. From 1992 to 1995, he was a Research Fellow with the University of Michigan, Ann Harbor. From 1995 to 2001, he was a Senior Research Scientist with the Bio-logic Systems Corporation, Mundelein, IL. He is currently a Research Scientist with the HST Biomedical Engineering Center, Harvard-MIT Division of Health Sciences and Technology, Massachusetts Institute of Technology, Cambridge. His research interests include physics, modeling of biological systems, artificial neural networks, and biological signal processing.

T. R. Gowrishankar received the B.E. degree in electronics engineering from Bangalore University, Bangalore, India, in 1986, the M.S. degree in electrical engineering from George Mason University, Fairfax, VA, in 1989 and the Ph.D. degree in medical physics from the University of Chicago, Chicago, IL, in 1996.

He is currently a Visiting Scientist with the HST Biomedical Engineering Center, Harvard-MIT Division of Health Sciences and Technology, Massachusetts Institute of Technology, Cambridge. He is also with Path Scientific, LLC, Carlisle, MA, a drug delivery company where he heads research and development. His research interests include transport in biological systems, drug delivery, and electrical injury.

James C. Weaver, photograph and biography not available at the time of publication.